AIAA JOURNAL
Vol. 42, No. 9, September 2004

Mode-Matching Strategies in Slowly Varying Engine Ducts

N. C. Ovenden* and S. W. Rienstra†
Eindhoven University of Technology, 5600 MB Eindhoven, The Netherlands

A matching method is proposed to connect the computational fluid dynamics (CFD) source region to the computational aeroacoustics propagation region of rotor–stator interaction sound produced in a turbofan engine. The method is based on a modal decomposition across three neighbouring axial interfaces adjacent to the matching interface. The modal amplitudes are determined by a least-squares fit. When slowly varying modes are taken, the interface may be positioned in a duct section of varying cross section. Furthermore, the spurious reflections back into the CFD domain, which result from imperfect reflection-free CFD boundary conditions, can be filtered out by including both left- and right-running modes in the matching. Although the method should be applicable to a wider range of acoustic models, it is implemented and favourably tested for the recently available relatively simple case of slowly varying modes in homentropic potential flow in lined ducts. Homentropic potential flow is a very relevant model for the inlet side and a good model for the bypass side if swirl or other types of vorticity are not dominant in the mean flow. By matching with density or pressure perturbations, any contamination of residual nonacoustical vorticity is avoided.

Nomenclature

A_μ	=	modal amplitudes
$\boldsymbol{a}$	=	vector of amplitudes
C	=	mean sound speed
c	=	sound speed
D	=	mean flow density
E	=	Bernoulli constant
F	=	mean mass flux through duct
k_μ	=	axial wave number
M	=	number of modes taken in each direction
$\mathcal{M}, \mathcal{N}, \mathcal{Q}$	=	square matrices
Ma	=	Mach number
m	=	circumferential wave number
N_μ, M_μ	=	slowly varying amplitude coefficients
n	=	integer
P	=	mean pressure
$\mathcal{P}_0, \mathcal{P}_1, \mathcal{P}_2$	=	computational fluid dynamics (CFD) pressure data at a single axial plane
p	=	pressure
$\boldsymbol{p}_0, \boldsymbol{p}_1, \boldsymbol{p}_2$	=	known vector obtained from CFD data
R_1, R_2	=	inner and outer duct walls
r	=	radial coordinate
s	=	entropy
t	=	time variable
U	=	mean axial velocity
u_μ	=	axial velocity of mode
$\boldsymbol{v}$	=	velocity vector
x, X	=	fast and slow axial coordinates
x_0, x_1, x_2	=	position of each matching plane
α_μ	=	radial wave number
γ	=	ratio of specific heats (constant)
ϵ	=	small parameter (multiple-scales theory)
θ	=	azimuthal coordinate
$\xi_\mu, \zeta_\mu, \chi_\mu$	=	basis functions
ρ	=	density
ϕ	=	velocity potential
ψ_μ	=	slowly varying eigenfunction
Ω	=	shaft frequency
ω	=	frequency, Helmholtz number

Subscripts

μ	=	mode index
∞	=	dimensional reference value

Superscript

$*$	=	complex conjugate

Introduction

COMPUTATIONALLY it is inefficient, and as yet practically impossible, to describe the sound field that is produced within a turbofan aeroengine duct, by rotor–stator interaction of fan and outlet guide vanes (OGVs), throughout the entire domain of interest by the same model.

In the aerodynamic regions of the source, that is, in the vicinity of fan, gap, and OGV (Fig. 1), the unsteady parts of all flow variables such as pressure, velocity, density, and possibly the thermodynamic variables are of the same order of magnitude as the steady (time-averaged) parts. The governing model is, therefore, nonlinear, time dependent, and rotational. It is described by some form of the compressible Navier–Stokes equations, possibly supplemented by a turbulence model. Under simplifying assumptions, such as lightly loaded fan blades, linear theory can be developed in the rotating frame of reference of the fan blades leading to predictions of the sound field produced by modal scattering.[1–7] However, in general cases, and particularly in the acoustically most critical case of heavy blade loading, the source model is mathematically so complicated that it can only be solved numerically by computational fluid dynamics (CFD) methods. On the other hand, in the acoustic regions of inlet and bypass duct and free field, the unsteady components are small compared to the steady (mean) flow. The model here may be split up into a steady description of the mean flow and a separate linear model for the perturbations. In addition, other simplifications that do not seriously affect the sound propagation may be justified, such as the absence of viscosity, vorticity and entropy variations for instance. The acoustic field may therefore be resolved by more

Presented as Paper 2003-3139 at the AIAA/CEAS 9th Aeroacoustics Conference, Hilton Head, SC, 12–14 May 2003; received 19 June 2003; revision received 8 April 2004; accepted for publication 8 April 2004.

*Postdoctoral Research Associate, Department of Mathematics and Computer Science; currently Research Fellow, Department of Mathematics, University College London, Gower Street, London, England WC1E 6BT, United Kingdom; nicko@math.ucl.ac.uk. Member AIAA.

†Associate Professor, Department of Mathematics and Computer Science; s.w.rienstra@tue.nl. Member AIAA.

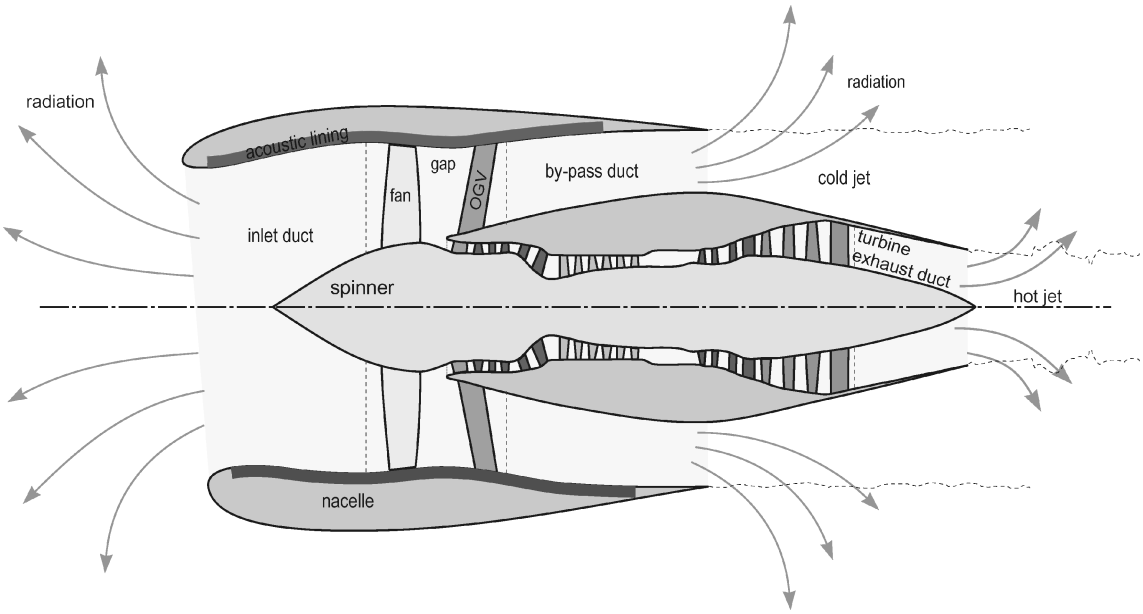

Fig. 1 Zones in a typical high-bypass-ratio turbofan engine.

efficient computational aeroacoustics (CAA) or (semi-) analytical techniques.

At the interface between both models, the source data from one is to be handed over to the other. Ideally, we would want to impose continuity of all variables and their derivatives at this interface. This is, however, not possible, and the differences between the models causes a matching problem across the interface where the following issues have to be faced.

First is the inconsistent field variables. Pressure, density, and velocity satisfy different equations in different models. Therefore, for example, a pressure and velocity field that are consistent in one model may be incompatible in another. We may have to choose which variable is preferred and cannot have both to be true.

Second are residual numerical errors and spurious reflections. The numerically obtained source field may have residual errors. In particular, the assumed reflection-free boundary condition is usually imperfect, and the field available from the CFD solution at the interface will in reality only partly transmit due to some reflections. This reflected part should be recognized; otherwise the resolved field will be an overestimation of reality.

Third are false reflections. When the difference in models is too great, this will in itself create false reflections that should not be included. This is an additional effect to the numerical reflections noted in the preceding paragraph. From our experience at present, the imperfect reflection-free boundary condition of the preceding paragraph appears to be the most significant.

Fourth is the false near field. A perfect matching of the acoustic field to the given field at the interface is, at least in one variable, always possible, but this solution will almost certainly contain an acoustic near field that is completely an artifact of the method. In terms of duct modes, this is the field associated with the exponentially decaying cutoff modes. If the duct near the matching interface is smooth and the field is linear, this part of the modal spectrum (the amplitudes of the cutoff modes) should be very small, because their origin lies at or near the rotor–stator blades and the nonlinear flow of the source region, not at the chosen matching interface. It is, however, impossible to quantify how small these modes should actually be, given the uncertainties of the source field. Therefore, we must try to limit these cutoff modes in a sensible way, but no more than necessary.

To translate the aerodynamic source data into their acoustic equivalents, the following two methods have been considered by Wilson in Refs. 8 and 9 and by Nijboer and Schulten (see Ref. 10) in a project commissioned by Rolls–Royce, plc., respectively.

First is use of wave splitting. If the interface is at a cross section of the duct that is perpendicular to the axis of symmetry, while the mean flow is axially constant, the field can be solved by a sum of modes. By the application of conditions of continuity of at least two variables (pressure and axial velocity, pressure and pressure gradient, depending on the acoustic model), a linear system can be created that defines the modal amplitudes. The advantage of the method is that it is relatively flexible to assumptions made about the source, so long as modes can be constructed. The disadvantages are that the duct has to be locally straight and that care must be taken that the two field variables are not inconsistent in the acoustic model, either because of the model differences or by the numerical discretization error.

Second is use of Ffowcs Williams–Hawkings integrals over the blades. It is argued that in the absence of shock waves associated to the rotor or stator blades, and in the absence of an important displacement effect due to the thickness of the blades, the dominating part of the source is the pressure distribution over the blades. These constitute a rotating distribution of dipoles, of which the radiated sound can be described by a Ffowcs Williams–Hawkings integral over the blades. The advantage of this method is that the pressure distribution can probably be relatively accurately determined. The disadvantages are that the Green's function in the duct is required for the solution, which is only explicitly available for simple ducts and mean flows, while effects such as the scattering of the rotor field by the stator, and vice versa, are not included. Indeed, for subsonic flow at relatively high Mach number ($Ma > 0.5$), the additional contribution from quadrapole sources ignored by this method is also significant at higher frequencies.[11]

Triple-Plane Pressure Matching Method

The preceding considerations brought us to the following matching method.

To be able to capture any type of source, we followed the idea of mode splitting at the interface, which allows us at the same time to remove any spurious reflections in the CFD data. We assume a circular symmetric annular duct, which is perfectly reasonable near the rotor. By using the slowly varying modes of Rienstra[12] and Rienstra and Eversman,[13] we are able to avoid the restriction of a straight duct section, and therefore, it is possible to match halfway along the spinner (in the inlet duct). In the present implementation, these modes are solutions of a homentropic potential flow model. The generalization to modes in flow with swirl[14–18] or ducts of arbitrary cross section[19] may be a next step, but is not done here yet.

The matching is done for a single variable to avoid any inconsistency. A convenient choice is the pressure because it is always available and is physically the most relevant variable for modeling

sound transmission. It is also (practically) not affected by vortical contamination, which is not dealt with by a potential flow model, as can be shown by writing the mass conservation equation in the form

$$\rho^{-1}\left(\frac{\partial}{\partial t}+\boldsymbol{v}\cdot\nabla\right)\rho=-\nabla\cdot\boldsymbol{v}$$

By linearizing about a steady mean flow, it is clear that any small (acoustic) density ρ perturbations convected by an $\mathcal{O}(1)$ mean flow only depend on the solenoidal part of the velocity $\boldsymbol{v}$. (This idea was originally raised by Wilson[8] for his second method.) For isentropic perturbations, the pressure p is merely algebraically related to the density by $\gamma p=\rho^{\gamma}$. Because matching of a single variable at a single axial plane is not enough to distinguish left- from right-running waves, the number of matching planes is extended to three. Two would be just enough, of course, but three offers some excess of information that allows, via a least-squares fit, a smoothing of errors and a better use of available information. Of course, one could take more matching planes than three; the idea remains exactly the same. Another advantage of a geometrically spread matching zone is the possibility of limiting the amplitudes of the cutoff modes in a simple and systematic way without resorting to ad hoc assumptions about the actual source locations (discussed later).

The slowly varying mean flow of the potential flow model is necessarily nearly uniform along a cross section. The axial velocity, mean density, and mean sound speed are, therefore, chosen such that their cross-sectional average is equal to the corresponding CFD mean flow component.

Finally, it may be noted that the present slowly varying modes are also valid for lined ducts, via the implementation of Myers's soft-wall boundary condition.[20] Hence, the matching interface may be chosen equally in either a hard-walled or lined duct section.

Equations for Ideal Fluid Motion

Because the matching interface refers to a jump in model, for example, from CFD to linearized potential flow, it is important to make clear what assumptions and approximations are made in the acoustic model that forms the basis for the present matching method. As noted before, the method is more general and can in principle be applied using any acoustic model that mathematically allows a representation of the solution by slowly varying modes. We start with the equations for a perfect gas and assume that (1) the acoustic variations are too rapid for heat conduction and (2) the viscous forces are negligible. (Reynolds number is large.) The problem is made dimensionless by scaling all spatial dimensions on a typical duct radius R_∞, the density ρ on some reference value ρ_∞, the velocity field $\boldsymbol{v}$ and sound speed c on a reference sound speed c_∞, time on R_∞/c_∞, and pressure p on $\rho_\infty c_\infty^2$. The governing equations are, subsequently,

$$\frac{\partial}{\partial t}\rho+\nabla\cdot(\rho\boldsymbol{v})=0,\qquad \rho\left(\frac{\partial}{\partial t}+\boldsymbol{v}\cdot\nabla\right)\boldsymbol{v}=-\nabla p$$

$$\left(\frac{\partial}{\partial t}+\boldsymbol{v}\cdot\nabla\right)s=0,\qquad \gamma p=\rho^{\gamma},\qquad c^2=\frac{\mathrm{d}p}{\mathrm{d}\rho}=\rho^{\gamma-1}$$

The third equation states that the entropy of a fluid particle remains constant as it is convected by the flow. When this constant is assumed to be the same for all streamlines, the flow is homentropic. If the flow is also irrotational (as in the inlet), we can introduce a velocity potential ϕ with $\boldsymbol{v}=\nabla\phi$ and integrate the momentum equation to obtain Bernoulli's equation,

$$\frac{\partial\phi}{\partial t}+\frac{1}{2}|\boldsymbol{v}|^2+\frac{c^2}{\gamma-1}=G(t)$$

where G is an unimportant function of time. The flow can now be split up into a mean flow plus small perturbations:

$$\boldsymbol{v}:=\boldsymbol{V}+\boldsymbol{v},\qquad p:=P+p$$

$$\phi:=\Phi+\phi,\qquad \rho:=D+\rho$$

and $c:=C+c$, although the sound speed perturbation plays no part in the subsequent analysis. After linearization, we obtain for the mean flowfield

$$\nabla\cdot(D\boldsymbol{V})=0,\qquad \gamma P=D^{\gamma},\qquad C^2=\gamma P/D=D^{\gamma-1}$$

$$\tfrac{1}{2}|\boldsymbol{V}|^2+C^2/(\gamma-1)=E$$

which is a constant, and for the acoustic field,

$$\frac{\partial}{\partial t}\rho+\nabla\cdot(D\nabla\phi+\rho\boldsymbol{V})=0$$

$$\frac{\partial}{\partial t}\phi+\boldsymbol{V}\cdot\nabla\phi+\frac{p}{D}=0,\qquad p=C^2\rho$$

which simplifies to solving

$$\left(\frac{\partial}{\partial t}+\boldsymbol{V}\cdot\nabla\right)\left[C^{-2}\left(\frac{\partial}{\partial t}+\boldsymbol{V}\cdot\nabla\right)\phi\right]=D^{-1}\nabla\cdot(D\nabla\phi)$$

Slowly Varying Modes

When a slowly varying duct, given by

$$R_1(X)\le r\le R_2(X),\qquad X=\varepsilon x$$

where ε is a small parameter, is the only cause of variation of the mean flow (an assumption), the mean flow variables depend essentially on the slow axial variable X, rather than on x, and application of the method of slow variation[21] leads to the asymptotic expansion

$$\boldsymbol{V}(X,r;\varepsilon)=U(X)\boldsymbol{e}_x+\varepsilon V(X,r)\boldsymbol{e}_r+\mathcal{O}(\varepsilon^2)$$

$$D(X,r;\varepsilon)=D(X)+\mathcal{O}(\varepsilon^2),\qquad C(X,r;\varepsilon)=C(X)+\mathcal{O}(\varepsilon^2)$$

$$P(X,r;\varepsilon)=P(X)+\mathcal{O}(\varepsilon^2)$$

where $\boldsymbol{e}_x$ and $\boldsymbol{e}_r$ are unit vectors in the axial and radial directions, respectively. The leading-order mean flowfield satisfies the equations

$$U(X)=F\Big/D(X)\left[R_2(X)^2-R_1(X)^2\right]$$

$$\tfrac{1}{2}U(X)^2+[1/(\gamma-1)]D(X)^{\gamma-1}=E$$

The two parameters F and E determine the entire mean flowfield and must be chosen to fit the CFD mean flow data as ideally as possible. The mean flow from the CFD must, therefore, be stripped of any swirling and vortical component to make the velocity nearly uniform axially. Given that πF is the mass flux through an axial plane, F can be found by determining the average mass flux of the mean flow at the three axial planes given. The Bernoulli constant E can be found by a similar averaging process of the mean density, or, indeed, the mean pressure or mean sound speed if they are regarded as more suitable.

Once a mean flow consistent with the acoustic model and close to the steady part of the CFD data has been derived, the acoustic field is Fourier decomposed in frequency and circumferential order. If $p(\boldsymbol{x},t)$ is periodic in time with period $2\pi/\Omega$, it can be written as

$$p(x,r,\theta,t)=\sum_{n=-\infty}^{\infty}\sum_{m=-\infty}^{\infty}p_m(x,r;n\Omega)\exp(in\Omega t-im\theta)$$

and each Fourier component is given by

$$p_m(x,r;n\Omega)=\frac{\Omega}{4\pi^2}\int_0^{2\pi}\int_0^{2\pi/\Omega}p(x,r,\theta,t)\times\exp(im\theta-in\Omega t)\,\mathrm{d}t\,\mathrm{d}\theta$$

Because in the rest of this paper we will deal with a single Fourier component $p_m(x,r;\omega)$ only, no explicit reference will be made to the circumferential order m or frequency ω dependence.

Each component is now a wave propagating in a slowly varying medium. (Both geometry and mean flow are to leading-order

functions of X only.) This can be approximated by an application of the Wentzel–Kramers–Brillouin (WKB) method (a variant of the method of multiple scales) where each radial mode is assumed to adapt itself to the varying surroundings, without any intermodal coupling.[12] The resulting field can then be written as a summation of left- and right-running modes in the following way:

$$p(x,r) = \sum_{\mu=-\infty}^{\infty} A_\mu \psi_\mu(X,r) \exp\left[-i\int^x k_\mu(\varepsilon\sigma)\,\mathrm{d}\sigma\right] \quad (1)$$

where $\mu = 0$ is excluded. The functions ψ_μ represent the basis functions for the right-running ($\mu > 0$) and left-running ($\mu < 0$) slowly varying pressure modes, which take the form[12]

$$\psi_\mu(X,r) = -i\,D(X)[\omega - k_\mu(X)U(X)]\{N_\mu(X)J_m[\alpha_\mu(X)r] + M_\mu(X)Y_m[\alpha_\mu(X)r]\} \quad (2)$$

where J_m and Y_m are Bessel functions of order m. The slowly varying radial eigenvalues α_μ are found from the hard or soft wall boundary condition,[20] and the axial eigenvalues k_μ can be subsequently derived for each α_μ via a slowly varying dispersion relation (with the correct sign convention of the square root for right, that is, $\mu > 0$, and left, that is, $\mu < 0$, running modes). The function N_μ is determined via a solvability condition[12] by assuming the solution to be in the form of an asymptotic expansion in ϵ. The other function M_μ is subsequently obtained from the ratio M_μ/N_μ, which is given by the hard or soft wall boundary condition.[20] These coefficients dictate entirely how the modal amplitude changes axially through the duct and are suitably normalized by making $\psi_\mu(X,r) = 1$ at the outer wall at a particular X station (usually one of the axial planes of the matching interface). Only near a cuton/cutoff transition (in hard-walled ducts)[22] or a near-cuton/cutoff transition (in soft-walled ducts)[23] the present approximation becomes invalid and should be replaced by a turning-point approximation. Therefore, in the presented approach these points should be avoided. For each mode, the only unknown remaining is the constant A_μ, which must be determined by matching to the CFD pressure data using the procedure described later.

Matching Method in Detail

Suppose that at three axial planes $x = x_0$, x_1, and x_2 (where $x_0 < x_1 < x_2$), representing the matching zone, the pressure $p(x,r)$ can be written by a finite sum of each plane's slowly varying basis functions as follows:

$$p(x,r) = \sum_{\mu=-M}^{M} A_\mu \psi_\mu(X,r) \exp\left[-i\int_{x_0}^x k_\mu(\varepsilon\sigma)\,\mathrm{d}\sigma\right] \quad (3)$$

Hence, given the Fourier decomposed (ω, m) component of the pressure data $\mathcal{P}_0(r)$ at $x = x_0$, $\mathcal{P}_1(r)$ at $x = x_1$, and $\mathcal{P}_2(r)$ at $x = x_2$, we can write

$$\sum_{\mu=-M}^{M} A_\mu \psi_\mu(X_0,r) = \mathcal{P}_0(r) \quad (4a)$$

$$\sum_{\mu=-M}^{M} A_\mu \psi_\mu(X_1,r) \exp\left[-i\int_{x_0}^{x_1} k_\mu(\varepsilon\sigma)\,\mathrm{d}\sigma\right] = \mathcal{P}_1(r) \quad (4b)$$

$$\sum_{\mu=-M}^{M} A_\mu \psi_\mu(X_2,r) \exp\left[-i\int_{x_0}^{x_2} k_\mu(\varepsilon\sigma)\,\mathrm{d}\sigma\right] = \mathcal{P}_2(r) \quad (4c)$$

Evidently, it will not be possible to find amplitudes A_μ that satisfy this overdetermined set of equations exactly. However, a best fit may be determined by a least-squares approach, although some care is needed to prevent exponentially large terms at the zone ends from unbalancing the least-squares minimization. Figure 2 shows two modes approaching the three-plane interface from either side. If these modes are cut off, $\mathrm{Im}(k_\mu) \neq 0$, then their respective amplitudes will decay exponentially as they pass through the interfaces. Hence, if they both have amplitudes of $\mathcal{O}(1)$ at the plane x_0, then at $x = x_2$ the amplitude of the right-running cutoff mode will be exponentially small and the amplitude of the left-running cutoff mode will be exponentially large. This leads to an imbalance in the minimization process, where the cutoff modal amplitudes are in general too large and the errors do not become spread evenly across all of the axial

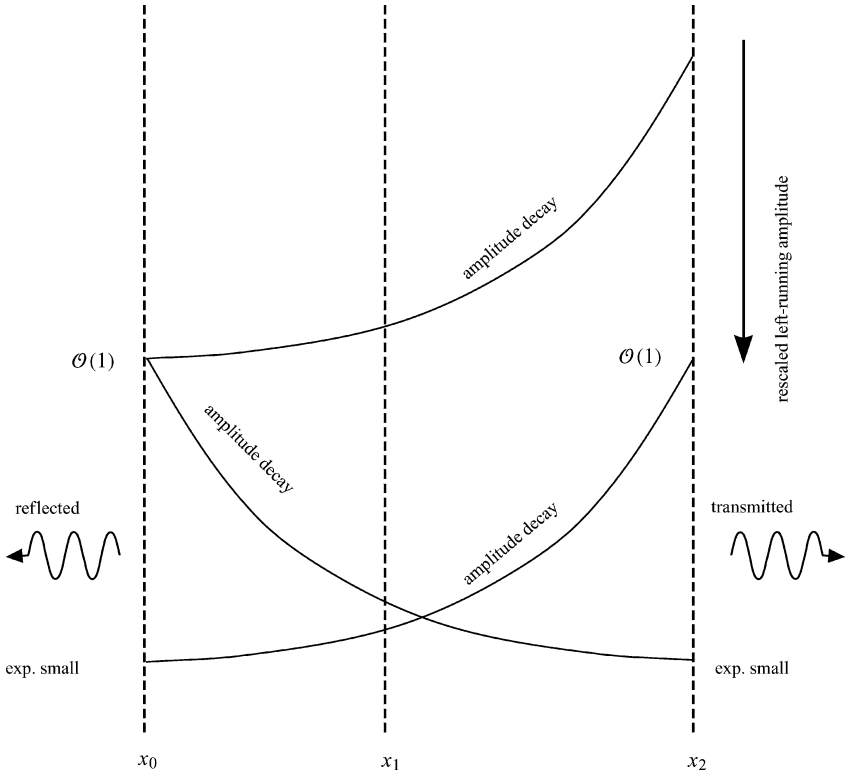

Fig. 2 Amplitude decay of cutoff modes across three axial planes.

planes. A typical consequence of this can be the appearance of oscillations or wiggles in the CAA pressure and velocity fields.

One satisfactory solution to the problem is to rescale the left- and right-running amplitudes and, reciprocally, rescale the corresponding basis functions, at whichever axial plane they take their maximum value in the least-squares procedure. In other words, they are rescaled to the axial plane nearest their apparent source. Hence, in Fig. 2, the amplitude of the left-running mode is rescaled to be $\mathcal{O}(1)$ at the end interface x_2 and to be exponentially small at $x = x_0$. Note that this does not involve any manual adaptation or postprocessing of the amplitudes. We just temporarily redefine amplitudes and basis functions such that the penalty in the least-squares method becomes effectively much greater for cutoff modes at the outer axial planes.

The bonus of this rescaling is that, while it limits the cutoff modes within the matching zone, it suppresses in a simple and systematic way the false near field created at the zone, but never suppresses more than what is actually present in reality.

The rescaling for the left-running amplitudes is conveniently given by introducing new amplitudes and basis functions as follows:

$$B_\mu = \begin{cases} A_\mu & \text{if} \quad \mu > 0 \\ A_\mu \exp\left[-i \int_{x_0}^{x_2} k_\mu(\varepsilon\sigma)\,\mathrm{d}\sigma\right] & \text{if} \quad \mu < 0 \end{cases} \tag{5a}$$

$$\xi_\mu(r) = \begin{cases} \psi_\mu(X_0, r) & \text{if} \quad \mu > 0 \\ \psi_\mu(X_0, r) \exp\left[-i \int_{x_2}^{x_0} k_\mu(\varepsilon\sigma)\,\mathrm{d}\sigma\right] & \text{if} \quad \mu < 0 \end{cases} \tag{5b}$$

$$\zeta_\mu(r) = \begin{cases} \psi_\mu(X_1, r) \exp\left[-i \int_{x_0}^{x_1} k_\mu(\varepsilon\sigma)\,\mathrm{d}\sigma\right] & \text{if} \quad \mu > 0 \\ \psi_\mu(X_1, r) \exp\left[-i \int_{x_2}^{x_1} k_\mu(\varepsilon\sigma)\,\mathrm{d}\sigma\right] & \text{if} \quad \mu < 0 \end{cases} \tag{5c}$$

$$\chi_\mu(r) = \begin{cases} \psi_\mu(X_2, r) \exp\left[-i \int_{x_0}^{x_2} k_\mu(\varepsilon\sigma)\,\mathrm{d}\sigma\right] & \text{if} \quad \mu > 0 \\ \psi_\mu(X_2, r) & \text{if} \quad \mu < 0 \end{cases} \tag{5d}$$

Consequently, a more balanced system is obtained:

$$\sum_{\mu=-M}^{M} B_\mu \xi_\mu(r) = \mathcal{P}_0(r) \tag{6a}$$

$$\sum_{\mu=-M}^{M} B_\mu \zeta_\mu(r) = \mathcal{P}_1(r) \tag{6b}$$

$$\sum_{\mu=-M}^{M} B_\mu \chi_\mu(r) = \mathcal{P}_2(r) \tag{6c}$$

The least-squares procedure can now be applied as follows. Multiply left- and right-hand sides of Eqs. (6) with the respective complex conjugated basis functions ξ_ν^*, ζ_ν^*, and χ_ν^*, and integrate across the duct to obtain

$$\sum_{\mu=-M}^{M} B_\mu \int_{R_1}^{R_2} \xi_\mu(r)\xi_\nu^*(r) r\,\mathrm{d}r = \int_{R_1}^{R_2} \mathcal{P}_0(r)\xi_\nu^*(r) r\,\mathrm{d}r \tag{7a}$$

$$\sum_{\mu=-M}^{M} B_\mu \int_{R_1}^{R_2} \zeta_\mu(r)\zeta_\nu^*(r) r\,\mathrm{d}r = \int_{R_1}^{R_2} \mathcal{P}_1(r)\zeta_\nu^*(r) r\,\mathrm{d}r \tag{7b}$$

$$\sum_{\mu=-M}^{M} B_\mu \int_{R_1}^{R_2} \chi_\mu(r)\chi_\nu^*(r) r\,\mathrm{d}r = \int_{R_1}^{R_2} \mathcal{P}_2(r)\chi_\nu^*(r) r\,\mathrm{d}r \tag{7c}$$

or in matrix form,

$$\mathcal{M}\boldsymbol{a} = \boldsymbol{p}_0, \qquad \mathcal{N}\boldsymbol{a} = \boldsymbol{p}_1, \qquad \mathcal{Q}\boldsymbol{a} = \boldsymbol{p}_2 \tag{8}$$

where

$$\{\mathcal{M}\}_{\nu\mu} = \int_{R_1}^{R_2} \xi_\mu(r)\xi_\nu^*(r) r\,\mathrm{d}r \tag{9a}$$

$$\{\mathcal{N}\}_{\nu\mu} = \int_{R_1}^{R_2} \zeta_\mu(r)\zeta_\nu^*(r) r\,\mathrm{d}r \tag{9b}$$

$$\{\mathcal{Q}\}_{\nu\mu} = \int_{R_1}^{R_2} \chi_\mu(r)\chi_\nu^*(r) r\,\mathrm{d}r \tag{9c}$$

$$\{\boldsymbol{p}_0\}_\nu = \int_{R_1}^{R_2} \mathcal{P}_0(r)\xi_\nu^*(r) r\,\mathrm{d}r \tag{9d}$$

$$\{\boldsymbol{p}_1\}_\nu = \int_{R_1}^{R_2} \mathcal{P}_1(r)\zeta_\nu^*(r) r\,\mathrm{d}r \tag{9e}$$

$$\{\boldsymbol{p}_2\}_\nu = \int_{R_1}^{R_2} \mathcal{P}_2(r)\chi_\nu^*(r) r\,\mathrm{d}r \tag{9f}$$

$$\{\boldsymbol{a}\}_\mu = B_\mu \tag{9g}$$

Note that the matrices $\mathcal{M}$, $\mathcal{N}$, and $\mathcal{Q}$ are not diagonal, even for hard-walled ducts, because each mode not only couples with itself, but also with its opposite-running counterpart. This leads to nonzero off-diagonal terms.

The least-squares approach aims to find a set of amplitudes $\boldsymbol{a}$ that minimizes the cost function

$$\|\mathcal{M}\boldsymbol{a} - \boldsymbol{p}_0\|^2 + \|\mathcal{N}\boldsymbol{a} - \boldsymbol{p}_1\|^2 + \|\mathcal{Q}\boldsymbol{a} - \boldsymbol{p}_2\|^2 \tag{10}$$

If we search for the vector $\boldsymbol{a}$ that minimizes cost function (10) and use the Hermitian property of $\mathcal{M}$, $\mathcal{N}$, and $\mathcal{Q}$, we get the following equation for $\boldsymbol{a}$:

$$(\mathcal{M}^2 + \mathcal{N}^2 + \mathcal{Q}^2)\boldsymbol{a} = \mathcal{M}\boldsymbol{p}_0 + \mathcal{N}\boldsymbol{p}_1 + \mathcal{Q}\boldsymbol{p}_2 \tag{11}$$

[Introduce the complex vectorial inner product $[\boldsymbol{x}, \boldsymbol{y}]$, which is equal to the ordinary inner product with $\boldsymbol{y}$ complex conjugated: $[\boldsymbol{x}, \boldsymbol{y}] = (\boldsymbol{x}, \boldsymbol{y}^*)$. Then the Hermitian property of $\mathcal{M}$ implies $[\mathcal{M}\boldsymbol{x}, \boldsymbol{y}] = [\boldsymbol{x}, \mathcal{M}^*\boldsymbol{y}] = [\boldsymbol{x}, \mathcal{M}\boldsymbol{y}]$. Each squared distance in cost function (10) becomes now like $\|\mathcal{M}\boldsymbol{a} - \boldsymbol{p}\|^2 = [\mathcal{M}\boldsymbol{a} - \boldsymbol{p}, \mathcal{M}\boldsymbol{a} - \boldsymbol{p}] = [\mathcal{M}^2\boldsymbol{a}, \boldsymbol{a}] - [\boldsymbol{a}, \mathcal{M}\boldsymbol{p}] - [\mathcal{M}\boldsymbol{p}, \boldsymbol{a}] + [\boldsymbol{p}, \boldsymbol{p}]$. If we vary around $\boldsymbol{a}$ by substituting $\boldsymbol{a} + \varepsilon\boldsymbol{b}$, we find for $\mathcal{O}(\varepsilon)$ that the variation of $\|\mathcal{M}\boldsymbol{a} - \boldsymbol{p}\|^2$ is $2\,\mathrm{Re}\,\{[\mathcal{M}^2\boldsymbol{a} - \mathcal{M}\boldsymbol{p}, \boldsymbol{b}]\}$. If we look for stationary values of cost function (10) for any vector $\boldsymbol{b}$, the result (11) for $\boldsymbol{a}$ is obtained]. This equation is easily solved by standard numerical techniques. The actual reflected amplitudes A_μ for $\mu < 0$ are then recovered from the resulting B_μ after the error minimization is completed.

To exclude the reflected modes in the preceding analysis is easy: all that is needed is to change the summation limits from

$$\sum_{\mu=-M}^{M} \quad \text{to} \quad \sum_{\mu=1}^{M}$$

and restrict the set of basis functions to the ones that are outgoing. The problem remains identical, except that the size of the vectors and matrices are M and $M \times M$, respectively, and for the case of hard walls the matrices are diagonal.

Testing the Triple-Plane Pressure Matching Strategy

The method was tested in a number of cases kindly provided by partners of the European collaborative project TurboNoiseCFD. We present here some examples supplied by Rolls–Royce, plc., and DLR, German Aerospace Research Center.

Rolls–Royce Fan/OGV in Bypass Duct

The Rolls–Royce CFD test data are based on a realistic engine geometry (Fig. 3) used in the TurboNoiseCFD project for investigating noise generated by rotor–stator interaction. Clearly, the engine duct geometry varies significantly along its axis, but in the region of the duct behind the OGVs, the duct is more or less parallel, with radial variations of $\mathcal{O}(10^{-4}$ m).

Rolls–Royce supplied data for 11 axial planes equally spaced between $x = 0.320$ m and $x = 0.360$ m at the stator-to-bypass-duct interface. Perturbation data were provided for a single frequency $\omega = 40.89$ (corresponding to two times the blade-passing frequency; 2BPF) and a single circumferential wave number $m = -13$. Observe in Fig. 4 that the mean flow has hardly any swirl but contains some vorticity (as expected). To conform to the acoustic model (homentropic potential flow), the mean flow must be stripped of its vorticity to create a uniform potential flow with the same mass flux; this is the model jump. The mean axial Mach number obtained is $Ma = 0.44$, and the average hub-to-tip ratio across the interfaces is 0.649. Solving the eigenvalue problem for the acoustic model predicts five cuton radial modes to be present. When the supplied CFD perturbation data are used, traditional wave-splitting methods, mentioned in the Introduction, of imposing continuity of pressure (ignoring reflections) and of imposing continuity of pressure and axial velocity, described as the $[P + V]$ method, were compared to the triple-plane pressure (TPP) matching strategy across all 11 axial locations. The amplitude coefficients A_μ for each radial mode were obtained from each of these methods and dimensionalized to give the mode's sound pressure level (SPL) at the outer casing. These results are presented in Figs. 5–8, and the main observations are described as follows.

When the matchings were performed, it soon became clear that there is significant vorticity contamination of the velocity field and just as significant reflections in this case. On the issue of reflections, the results in Fig. 5 for the TPP method, for instance, indicate that

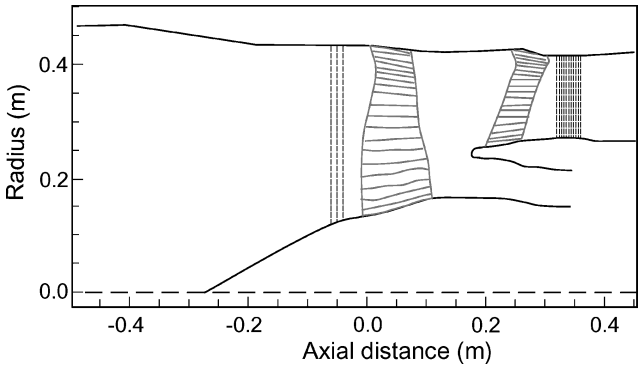

Fig. 3 Fan/OGV test case engine geometry.

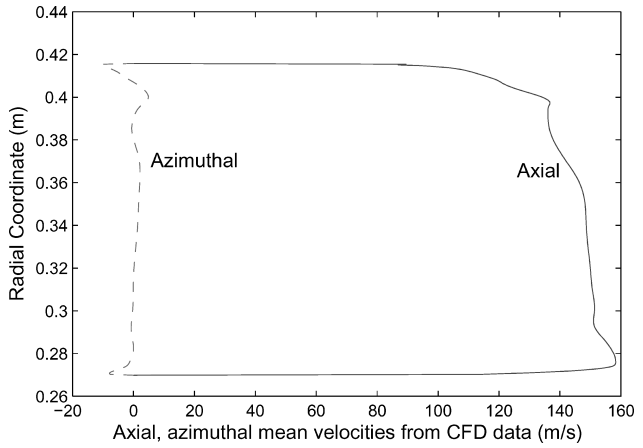

Fig. 4 Bypass fan/OGV test case; mean flow profiles at $x = 0.340$ m: ——, axial and · · · ·, azimuthal.

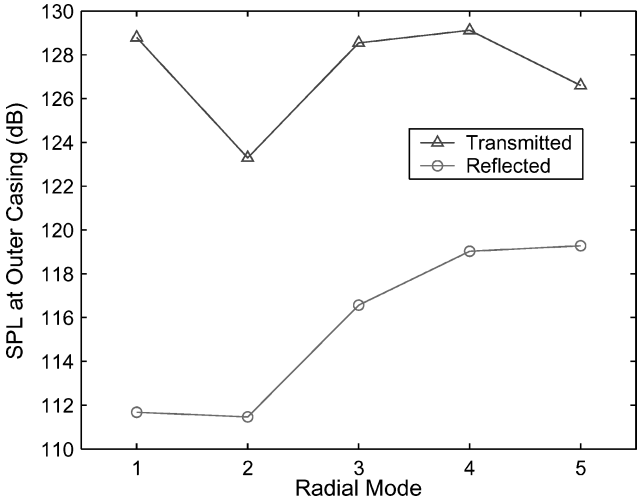

Fig. 5 Bypass fan/OGV test case; transmitted and reflected modal amplitudes (SPL) at the outer casing predicted by the TPP matching method at $x = 0.348$ m.

the reflected amplitudes of the cuton modes are about 20% of the amplitude of their transmitted counterparts. Matching without reflections in this case, therefore, leads to a significant overestimation (as expected) of the transmitted acoustic field.

As mentioned earlier, unsteady perturbations can be split into a solenoidal (acoustic) part and a vortical part. These are only weakly coupled in the almost uniform mean flow, and the vortical part of the pressure field is so weak that vorticity is practically only present in the velocity field. A potential flow cannot absorb the vortical part. Hence, when only the pressure is considered, the acoustic model ignores the vortical part and deals just with the solenoidal part of the velocity field $\nabla\phi$. For this test case, the magnitude of the vortical part of the flowfield compared to the acoustical (solenoidal) part can be assessed by reconstructing solenoidal axial velocity profiles from the matched modal amplitudes using the acoustic model and comparing these to the original CFD data. In the homentropic potential flow model, the irrotational axial velocity $(\partial/\partial x)\phi$ can be obtained from the axial velocity modes $\{u_\mu\}$ that correspond directly to the pressure modes of form (2). To the order of the approximation, the axial velocity modes are given by

$$u_\mu(X, r) = \frac{k_\mu(X)\psi_\mu(X, r)}{D(X)[\omega - U(X)k_\mu(X)]} \tag{12}$$

To demonstrate one example, TPP matching was applied to the CFD pressure data at the three axial planes $x = 0.340$ m, $x = 0.344$ m, and $x = 0.348$ m, and then the acoustic modes were summed to reconstruct the pressure and axial velocity profiles at the central axial plane $x = 0.344$ m (for the current frequency and circumferential wave number of interest). These are shown in Fig. 6 vs the original CFD data (nondimensionalized). The pressures of both CFD and modal solutions match exactly as one would expect, with a very slight discrepancy close to the inner wall. However, the most striking observation is that the modes obtained from the TPP strategy, which uses no velocity information from CFD, predicts the solenoidal axial velocity profile to be almost 1/10th of the magnitude of the original CFD profile. Although some of the error may be due to numerical noise, the most obvious explanation must be that the CFD axial velocity contains a significant (indeed dominant) vortical part, which does not contribute physically to the pressure field.

The observation that the vortical part of the axial velocity perturbations is greater than the solenoidal part naturally affects the accuracy of the traditional $[P + V]$ wave splitting methods significantly. The reason for this is that the $[P + V]$ wave splitting assumes the velocity field to be entirely (or at least mainly) solenoidal. Evidence of the resulting errors can be seen in the transmitted modal SPL at the outer casing derived by applying the $[P + V]$ wave splitting at

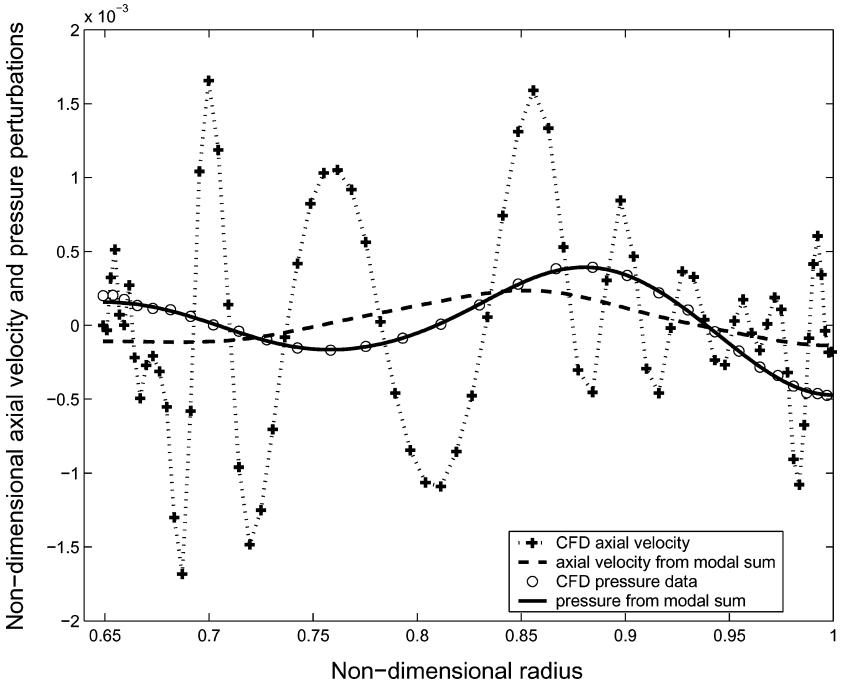

Fig. 6 Bypass fan/OGV test case; axial velocity and pressure perturbations obtained from the TPP matching and reconstructed using the homentropic potential flow model vs original CFD data at $x = 0.344$ m.

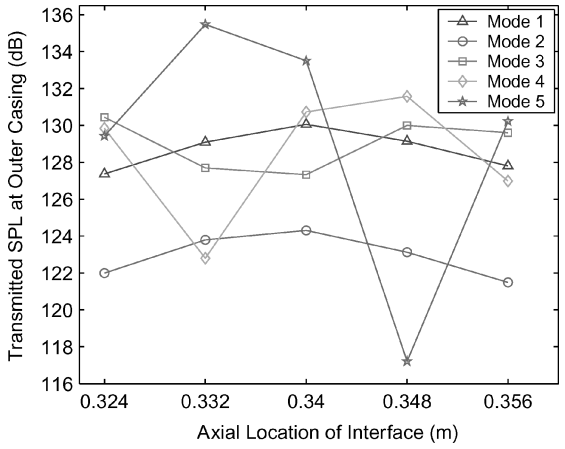

Fig. 7 Bypass fan/OGV test case; amplitudes (SPL) at the outer casing of the transmitted radial modes predicted by traditional $[P + V]$ wave splitting methods at five different axial locations.

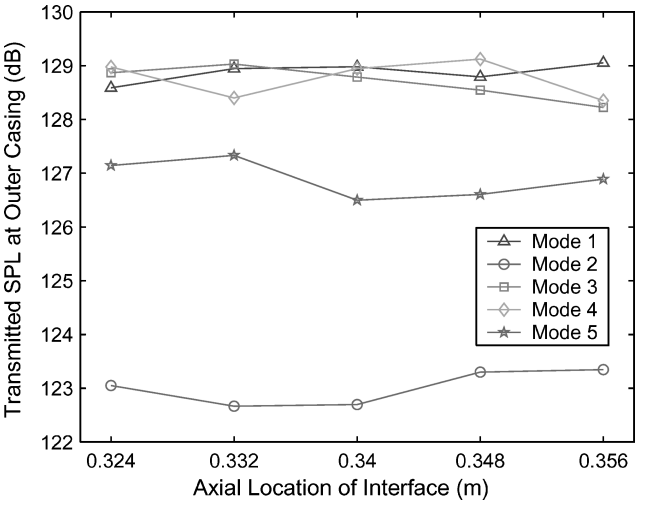

Fig. 8 Bypass fan/OGV test case; amplitudes (SPL) at the outer casing of the transmitted radial modes predicted by the TPP matching method at five different axial locations.

five different axial locations shown in Fig. 7. Given that the amplitude coefficients A_μ of the cuton modes should be constant in the homentropic potential flow acoustic model, the amplitudes obtained from the traditional wave splitting method show an enormous variability, even to the order of 10–15 dB for the fourth and fifth radial modes. Indeed, the resolution of the higher-order cuton modes appears to be strongly affected by the vorticity contamination.

The comparison of the $[P + V]$ wave splitting modal amplitudes to the almost constant transmitted amplitudes, with differences much less than 1 dB, obtained by the TPP matching method (Fig. 8) demonstrates strong proof of the superior ability of the TPP matching method to capture and extract the acoustically behaving part of such a complicated CFD solution extremely well. The TPP matching method, in effect, has not only matched the data but synchronized the acoustic field of the CFD and homentropic potential flow model, leading to a greater confidence that the model jump is actually not too severe in this case.

As a final comparison of matching in the bypass duct case (Fig. 9), another set of CFD data produced for the same bypass geometry

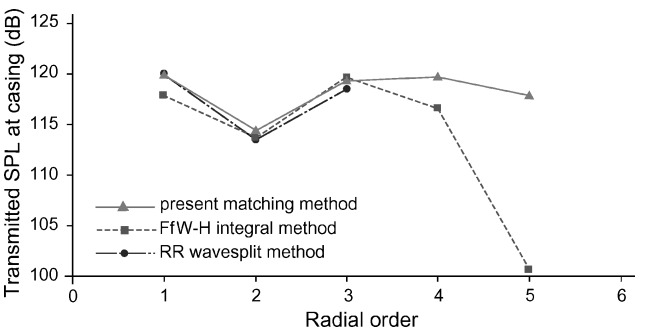

Fig. 9 Bypass fan/OGV test case. Comparison of the TPP matching method with a Rolls–Royce in-house wave splitting method and the acoustic analogy approach of Ffowcs Williams–Hawkings.

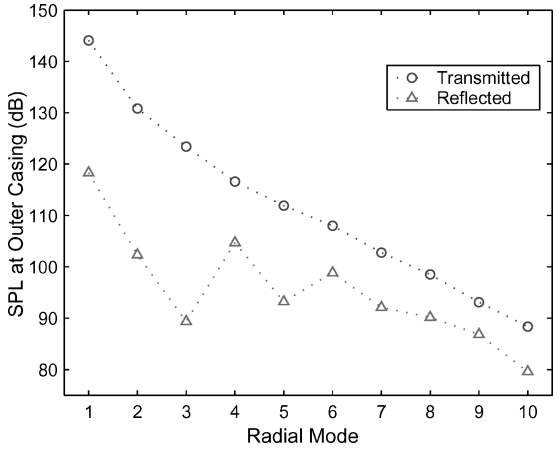

Fig. 10 Inlet test case; transmitted and reflected model amplitudes (SPL) at the outer casing from TPP matching.

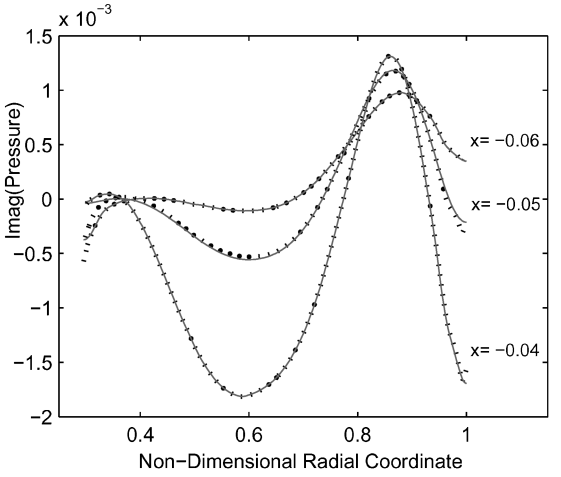

Fig. 11 Inlet test case; comparison at all three axial planes: · · · ·, CFD imaginary pressure data and ——, solution from the first 50 radial modes derived from the TPP matching method.

was matched using the TPP matching method and compared to a Rolls–Royce in-house wave splitting method[8,9] and the acoustic analogy approach of Ffowcs Williams–Hawkings (FW–H)[10]; both of these methods were briefly described in the Introduction. Very good agreement is obtained for the first three radial modes in all cases, although the agreement is nowhere near as good for the fourth and fifth radial modes. Indeed, the in-house wave splitting method is unable to resolve these higher-order radial modes, possibly due to the strong vorticity effects described earlier.

Although the FW–H method is able to resolve the fourth and fifth modal amplitudes, they are likely to be underestimated for the following reason. The FW–H method is not based directly on the field that is actually present, but on the field reconstructed from the unsteady pressure distribution from dipole sources over the blades. Any contributory effects due to quadrapole sources, nonlinear flow near the blades, turbulence, or scattering from either the rotor or stator blades are not accounted for by FW–H. These additional sources may well occur over scales much smaller than a single blade and, thus, would excite the higher-order modes predominately.

The TPP matching method does not suffer from such difficulties. When the consistency of our results is considered, it is reasonable to postulate that the TPP result is probably the most accurate in obtaining the fourth and fifth modal amplitudes.

DLR Inlet Matching on a Spinner

For exactly the same engine geometry as the Rolls–Royce case (Fig. 3), another partner in the TurboNoiseCFD project, DLR, Germany, was able to supply sets of CFD data at three axial planes for inlet-duct matching (upstream of the fan in Fig. 3). The case presented here is at a frequency of $\omega = 21.5$ (1BPF) and circumferential wave number $m = -26$, where the average axial Mach number is taken to be $Ma = 0.35$. This test case enabled us not only to tackle the difficult task of matching on the spinner, where the axial variation of the duct is highly significant, but also to examine the ability of the TPP matching method to deal with cutoff modes correctly. (There are no cuton radial modes in this case.) Data were supplied at axial planes $x = -0.06$ m, $x = -0.05$ m, and $x = -0.04$ m, and the transmitted and reflected modal amplitudes (SPL) at the outer casing of the plane farthest upstream are shown in Fig. 10. Modal reflections appear to be fairly negligible in this case (20 dB lower than the transmitted amplitudes for lower radial orders), and the modal amplitudes drop smoothly with increasing radial order, in line with physical expectations.

Figure 11 shows a comparison of the CFD pressure data (imaginary part) with that derived from our homentropic potential flow model, using the obtained modal amplitudes. The agreement appears to be excellent, with both CFD and analytical models capturing the exponential decay of the sound field away from the source.

Conclusions

To make progress in the prediction of turbomachinery noise by direct calculation with CFD methods of the noise sources, such as rotor–stator interaction between fan and OGVs or between compressor and turbine stages, it is necessary to decouple the noise generation from the propagation effects. Otherwise, the available computational resources will not be sufficient for many years to come.

By our TPP matching method, we have shown that it is possible to take the CFD noise field from planes in the vicinity of the CFD domain boundaries and extract in a robust manner the information required to input to CAA or analytical models, which are designed to describe the propagation and radiation processes more efficiently.

The method is both robust and flexible, because it is based on a least-squares fit that in principle allows the matching of any flow variable at any number of planes. A subtle scaling of the amplitudes proves to be sufficient to suppress the exponential coupling of cutoff modes between the matching zone ends and, at the same time, limits in a simple and systematic manner the occurrence of the false near field that is bound to occur when a pressure distribution at a single interface acts as an acoustic boundary condition.

By use of slowly varying modes, there is no geometrical restriction to the location of the interface. It is indeed possible to apply the matching at any diverging or converging part of the duct. Perhaps the only locations that should be avoided for matching are close to areas where either cuton/cutoff transition (in hard-walled ducts) or near cuton/cutoff transition (in lined ducts) of a mode may occur.[22,23]

Acknowledgments

This work was supported by the TurboNoiseCFD European collaborative project (EU Technical Officer Per Kruppa and Coordinator Brian Tester). We thank all partners for their contributions and comments in the development of this work. We gratefully acknowledge Rolls–Royce, plc. (RR) (United Kingdom), and DLR, German Aerospace Research Center (Germany), for supplying the computational fluid dynamics data presented here, and especially John Coupland (RR) for the comparison with the National Aerospace Laboratory (The Netherlands) Ffowcs Williams–Hawkings integral method of Nijboer and Schulten and the wave splitting method of Alec Wilson (RR). Finally, we thank the referees for their comments and suggestions.

References

[1]Atassi, H. M., "Unsteady Aerodynamics of Vortical Flows: Early and Recent Developments," *Aerodynamics and Aeroacoustics*, World Scientific, Singapore, 1994, pp. 121–172.

[2]Atassi, H. M., Ali, A. A., Atassi, O. V., and Vinogradov, I. V., "Scattering of Incident Disturbances by an Annular Cascade in a Swirling Flow," *Journal of Fluid Mechanics*, Vol. 499, 2004, pp. 111–138.
[3]Namba, M., "Lifting Surface Theory for a Rotating Subsonic or Transonic Blade Row," Aeronautical Research Council, Repts. and Memoranda No. 3740, London, 1972.
[4]Schulten, J. B. H. M., "Vane Sweep Effects on Rotor/Stator Interaction Noise," *AIAA Journal*, Vol. 35, 1997, pp. 945–951.
[5]Peake, N., and Kerschen, E. J., "Influence of Mean Loading on Noise Generated by the Interaction of Gusts with a Flat-Plate Cascade: Upstream Radiation," *Journal of Fluid Mechanics*, Vol. 347, 1997, pp. 315–346.
[6]Sijtsma, P., Rademaker, E. R., and Schulten, J. B. H. M., "Experimental Validation of Lifting Surface Theory for Rotor–Stator Interaction Noise Generation," *AIAA Journal*, Vol. 36, No. 6, 1998, pp. 900–906.
[7]Namba, M., and Schulten, J. B. H. M.,"Numerical Results of Lifting Surface Theory—Cat. 4 Benchmark," *Proceedings of the Third Computational Aeroacoustics (CAA) Workshop on Benchmark Problems*, edited by M. D. Dahl, Ohio Aerospace Inst., Cleveland, OH, 1999; also NASA CP-2000-209790, Aug. 2000, pp. 73–85; also National Aerospace Lab., NLR-TP-2000-013, Amsterdam, Jan. 2000.
[8]Wilson, A. G., "A Method for Deriving Tone Noise Information from CFD Calculations on the Aeroengine Fan Stage," NATO RTO-MP-079(1), Neuilly-sur-Seine, France, Feb. 2003, Paper (SYA)-3.
[9]Wilson, A. G., "Application of CFD to Wake/Aerofoil Interaction Noise—A Flat Plate Validation Case," AIAA Paper 2001-2135, May 2001.
[10]Nijboer, R. J., "BLAIR—BLade Acoustic Integration Routine: An Acoustic Radiation Code," National Aerospace Lab./NLR, NLR-CR-2001-165, Amsterdam, April 2001.
[11]Atassi, H. M., Fang, J., and Patrick, S. M., "Direct Calculation of Sound Radiated from Bodies in Nonuniform Flows," *Journal of Fluids Engineering*, Vol. 115, 1993, pp. 573–579.
[12]Rienstra, S. W., "Sound Transmission in Slowly Varying Circular and Annular Lined Ducts with Flow," *Journal of Fluid Mechanics*, Vol. 380, 1999, pp. 279–296.
[13]Rienstra, S. W., and Eversman, W., "A Numerical Comparison Between Multiple-Scales and FEM Solution for Sound Propagation in Lined Flow Ducts," *Journal of Fluid Mechanics*, Vol. 437, 2001, pp. 367–384.
[14]Cooper, A. J., and Peake, N., "Propagation of Unsteady Disturbances in a Slowly Varying Duct with Mean Swirling Flow," *Journal of Fluid Mechanics*, Vol. 445, 2001, pp. 207–234.
[15]Golubev, V. V., and Atassi, H. M., "Sound Propagation in an Annular Duct with Mean Potential Swirling Flow," *Journal of Sound and Vibration*, Vol. 198, No. 5, 1996, pp. 601–616.
[16]Golubev, V. V., and Atassi, H. M., "Acoustic-Vorticity Waves in Swirling Flows," *Journal of Sound and Vibration*, Vol. 209, No. 2, 1998, pp. 203–222.
[17]Tam, C. K. W., and Auriault, L., "The Wave Modes in Ducted Swirling Flows," *Journal of Fluid Mechanics*, Vol. 371, 1998, pp. 1–20.
[18]Nijboer, R. J., "Eigenvalues and Eigenfunctions of Ducted Swirling Flows," AIAA Paper 2001-2178, May 2001.
[19]Rienstra, S. W., "Sound Propagation In Slowly Varying Lined Flow Ducts Of Arbitrary Cross Section," *Journal of Fluid Mechanics*, Vol. 495, 2003, pp. 157–173.
[20]Myers, M. K., "On the Acoustic Boundary Condition in the Presence of Flow," *Journal of Sound and Vibration*, Vol. 71, No. 3, 1980, pp. 429–434.
[21]Van Dyke, M., "Slow Variations in Continuum Mechanics," *Advances in Applied Mechanics*, Vol. 25, Academic Press, Orlando, FL, 1987, pp. 1–45.
[22]Rienstra, S. W., "Cut-On, Cut-Off Transition of Sound in Slowly Varying Flow Ducts," *Aerotechnica — Missili e Spazio*, Special Issue in Memory of Prof. D. G. Crighton, Vol. 79, Nos. 3-4, 2000, pp. 93–97.
[23]Ovenden, N. C., "Near Cut-On/Cut-Off Transition in Lined Ducts with Flow," AIAA Paper 2002-2445, June 2002.

H. Atassi
Associate Editor